

Differentially Private 2D Human Pose Estimation

Kaushik Bhargav Sivangi
University of Glasgow
Glasgow, United Kingdom
Kaushik.Sivangi@glasgow.ac.uk

Paul Henderson
University of Glasgow
Glasgow, United Kingdom
Paul.Henderson@glasgow.ac.uk

Idris Zakariyya
University of Glasgow
Glasgow, United Kingdom
Idris.Zakariyya@glasgow.ac.uk

Fani Deligianni
University of Glasgow
Glasgow, United Kingdom
Fani.Deligianni@glasgow.ac.uk

Abstract

Human pose estimation (HPE) has become essential in numerous applications including healthcare, activity recognition, and human-computer interaction. However, the privacy implications of processing sensitive visual data present significant deployment barriers in critical domains. While traditional anonymization techniques offer limited protection and often compromise data utility for broader motion analysis, Differential Privacy (DP) provides formal privacy guarantees but typically degrades model performance when applied naively. In this work, we present the first differentially private 2D human pose estimation (2D-HPE) by applying Differentially Private Stochastic Gradient Descent (DP-SGD) to this task. To effectively balance privacy with performance, we adopt Projected DP-SGD (PDP-SGD), which projects the noisy gradients to a low-dimensional subspace. Additionally, we adapt TinyViT, a compact and efficient vision transformer for coordinate classification in HPE, providing a lightweight yet powerful backbone that enhances privacy-preserving deployment feasibility on resource-limited devices. Our approach is particularly valuable for multimedia interpretation tasks, enabling privacy-safe analysis and understanding of human motion across diverse visual media while preserving the semantic meaning required for downstream applications. Comprehensive experiments on the MPII Human Pose Dataset demonstrate significant performance enhancement with PDP-SGD achieving 78.48% PCKh@0.5 at a strict privacy budget ($\epsilon = 0.2$), compared to 63.85% for standard DP-SGD. This work lays foundation for privacy-preserving human pose estimation in real-world, sensitive applications.

CCS Concepts

• **Computing Methodologies** → **Activity recognition and understanding**; • **Security and privacy** → *Privacy protections*.

Permission to make digital or hard copies of all or part of this work for personal or classroom use is granted without fee provided that copies are not made or distributed for profit or commercial advantage and that copies bear this notice and the full citation on the first page. Copyrights for components of this work owned by others than the author(s) must be honored. Abstracting with credit is permitted. To copy otherwise, or republish, to post on servers or to redistribute to lists, requires prior specific permission and/or a fee. Request permissions from permissions@acm.org.

© XX Copyright held by the owner/author(s). Publication rights licensed to ACM.
ACM ISBN 978-1-4503-XXXX-X/2018/06
<https://doi.org/XXXXXXX.XXXXXXX>

Keywords

2D Human Pose Estimation, Differential Privacy

ACM Reference Format:

Kaushik Bhargav Sivangi, Idris Zakariyya, Paul Henderson, and Fani Deligianni. XX. Differentially Private 2D Human Pose Estimation. In *Proceedings of* . ACM, New York, NY, USA, 9 pages. <https://doi.org/XXXXXXX.XXXXXXX>

1 Introduction

Human pose estimation (HPE) represents a fundamental multimedia interpretation task that transforms raw visual content into structured representations of human positioning and movements. This sophisticated conversion of visual data into anatomically meaningful keypoint configurations enable numerous high impact applications in healthcare, activity recognition, human-computer interaction, sports analysis and video games [6, 32, 36, 38, 48].

As these multimedia systems are increasingly integrated into sensitive environments such as hospitals and homes, protecting user privacy has become a critical concern [1]. HPE systems that capture and process raw images pose significant privacy risks in two key ways: first, the raw images themselves contain sensitive personal information that could be exposed during collection and processing [59]; second, even trained models can inadvertently reveal information about individuals in training data when subjected to sophisticated privacy attacks such as model inversion or membership inference techniques [18, 26, 56]. For instance, an adversary can exploit a model's weights [19] or gradients [21] to reconstruct distinctive physical characteristics of patients or sensitive contextual information, such as the patient's home environment from the private training dataset [26]. This reconstruction could potentially identify individuals with specific medical conditions and reveal that they received treatment at a particular facility during the model's training period, thereby compromising both medical confidentiality and location privacy.

Previous approaches to privacy preservation in HPE have focused primarily on data anonymization techniques, such as blurring, pixelation, and template-based shape modeling [4, 22, 42]. While these methods provide some level of privacy protection, they are often task-specific and can severely compromise the utility of the data for broader analysis. For instance, anonymization that removes facial features might preserve basic joint position information but destroy crucial clinical indicators needed for stress level assessment or abnormal motion pattern detection [7]. Furthermore, these

methods typically lack theoretical privacy guarantees and remain vulnerable to more sophisticated attacks, limiting their applicability in highly sensitive contexts [56]. Moreover, these approaches do not address the inherent vulnerability of neural networks to memorization attacks that can reconstruct training data [19]. This limitation significantly limits the potential to share models trained in sensitive multimedia datasets in the wider research community and clinical applications.

The inherent tension between improving model utility and ensuring robust privacy preservation represents a challenging research problem [3, 17, 61] that has not been adequately explored in the context of HPE. Differential privacy (DP) offers a promising framework to address these concerns by providing mathematical guarantees against data leakage [2, 15, 16, 20]. However, implementing DP in deep learning models, particularly through Differentially Private Stochastic Gradient Descent (DP-SGD)[2], typically results in substantial performance degradation that can render models impractical for real-world applications [11, 54]. This degradation is problematic in vision tasks such as HPE, where the utility of the model relies on maintaining fine-grained spatial precision.

In this paper, we address the fundamental challenge of balancing the trade-off between privacy protection and model utility in HPE. Our work makes three significant contributions:

- We present the first systematic application of DP-SGD to the Human Pose Estimation task. We empirically establish strong privacy-preserving baselines using DP-SGD on the MPII human pose dataset [41], and demonstrate the trade-off between utility and privacy in HPE models.
- We successfully integrate Projected DP-SGD (PDP-SGD) to enhance the privacy-utility tradeoff in 2D-HPE. By projecting noisy gradients onto a low-dimensional subspace learned from a public dataset, we reduce noise amplification from DP and improve convergence, providing a more practical solution for tight privacy budgets.
- We develop a novel lightweight and efficient HPE architecture based on TinyViT with a coordinate classification head, specifically designed to be compatible with differential privacy. This lightweight, DP-compatible architecture offers improved performance with reduced model size and serves as strong backbone for DP-optimized pose estimation, making privacy-preserving deployment more feasible on resource-limited devices.

Our experimental results on the MPII dataset [41] demonstrate that the proposed method achieves competitive performance compared to non-private baselines, with reasonable accuracy degradation at practical privacy budgets. Our projection-enhanced DP-SGD approach for HPE consistently improves pose estimation accuracy by up to 20% at strict privacy budgets ($\epsilon = 0.2$), with the most substantial gains observed when using moderate gradient clipping thresholds ($C=0.1$, $C=1.0$). Fine-tuning pretrained models with carefully selected clipping norms further enhances performance over training from scratch. These results establish a practical pathway for deploying privacy-preserving HPE in sensitive domains. While our framework builds on existing techniques such as DP-SGD, we demonstrate its empirical viability for structured prediction tasks like HPE, addressing a gap in privacy-preserving computer vision.

2 Related Work

2.1 Markerless 2D Human Pose Estimation

Markerless 2D-HPE identifies anatomical keypoints in images without physical markers, thus playing a fundamental role in human motion analysis for several applications in healthcare and activity recognition [10, 13]. Although traditional heatmap methods originally based on CNN architectures [6, 12, 27, 44, 47, 50, 57] and later leveraging vision-based transformers [31, 33, 37, 51, 55] achieved state-of-the-art performance, they suffer from quantization errors and usually result in large cumbersome networks. Regression approaches offer faster, end-to-end solutions but with reduced accuracy [30, 40, 45, 60]. Recently, a coordinate classification approach has been proposed to address these limitations by treating pose estimation as a classification problem with discretized coordinates [32]. This method achieved state-of-the-art performance while maintaining computational efficiency. Knowledge distillation techniques [8, 34, 52, 58] have been also applied to enhance the efficiency of HPE with significantly less model parameters and inference speed by transferring knowledge from large heatmap based models to smaller architectures.

2.2 Privacy Preservation in 2D-Human Pose Estimation

Protecting the privacy of users is of paramount importance in all real-world applications and a challenging task for human pose estimation, which depends on high-quality images. Both trained models and training datasets can become vulnerable targets for attacks in modern multimedia systems. Recent research has demonstrated that adversaries can successfully reconstruct substantial portions of private training data solely by analyzing the parameters of a trained neural network [19, 26]. For these reasons, in critical applications, data sharing initiatives provide limited information, such as the location of limb joints and depth images [25]. This restricted access prevents the analysis of crucial clinical indicators that require body shape or facial information to detect levels of stress and identify abnormal motion patterns. In practice, most platforms implement rudimentary privacy protection based on face de-identification with blurring and pixelation [42]. Some approaches to protecting people's privacy have evolved from basic techniques to more sophisticated methods, although significant challenges persist. Early work by [22] employed skin removal and template-based shape modeling, which compromised clinical utility despite privacy benefits. Recently, more sophisticated methods have been developed. In [23], an end-to-end framework is proposed that integrates an optimized optical encoder with a CNN decoder, incorporating a visual privacy protection layer to degrade private attributes while preserving essential features. These methods lack theoretical privacy guarantees and remain vulnerable to reconstruction attacks [56]. Furthermore, they are fine-tuned for a specific task, which implies that extracting additional useful information from the data might not be possible.

2.3 Utility vs privacy with DP optimization

DP-SGD is one of the most common methods in developing privacy-preserved deep learning models because of the strong privacy guarantees compared to data-independent methods and its ability to scale to large datasets [15, 20]. In DP-SGD the process involves clipping the gradients first to bound the maximum norm of individual gradients and subsequently adding Gaussian noise. Clipping the gradients ensures that the gradients' sensitivity is bounded so that any single data point would have very limited influence [29]. In this way, DP is maintained by preventing a single data point disproportionately influencing the deep learning model.

However, there is a trade-off between privacy and utility in DP settings that can compromise the ability to develop privacy-preserved HPE algorithms that would be useful in practice [3]. The performance of DP-SGD has been shown to depend on the smoothness of the loss function [46] and the dimension of the gradient [17, 61]. It has also been shown that if the loss function lacks Lipschitz continuity, the performance of DP-SGD critically depends on carefully selecting an appropriate clipping threshold; otherwise, performance will not improve significantly, regardless of the amount of training data or iterations [17]. To our knowledge, in the context of preserving the privacy of the models in HPE, there is no work that studies the utility-privacy trade-off.

3 Methodology

Towards our goal of exploring the intersection of privacy and utility in HPE, we design a modular framework for differentially private 2D HPE. Our approach assumes access to a public dataset, used for pretraining, and a private dataset on which the model is subjected to formal DP constraints. At the core, we employ DP-SGD with calibrated clipping and noise addition, aligning with the structured nature of pose outputs (Sec. 3.1). To address the degradation of utility under DP-SGD, we incorporate Projected DP-SGD (PDP-SGD) [61], which projects the noisy gradients associated with private set onto a gradient subspace derived from a subset of public data (Sec. 3.3). Finally, we instantiate our framework using a novel DP-compatible architecture based on the compact TinyViT backbone with a coordinate classification head (Sec. 3.4).

3.1 Differential Privacy (DP)

To ensure privacy preservation in any application, it is essential to establish a quantifiable definition of privacy. DP provides a rigorous mathematical framework to quantify the privacy guarantees of a system [20]. Specifically, in the context of databases, DP measures how much the inclusion or exclusion of a single data point can influence the output of a randomized algorithm [15].

Consider two neighboring datasets, i.e., datasets that differ by only a single sample. The level of DP achieved by a randomized algorithm \mathcal{M} is defined as follows:

Definition 1: (ϵ, δ) -DP A randomized algorithm \mathcal{M} with domain \mathcal{D} and range \mathcal{R} is said to be (ϵ, δ) -DP if, for any subset $S \subseteq \mathcal{R}$ and for any neighboring datasets $d, d' \in \mathcal{D}$, the following condition holds:

$$\mathbb{P}[\mathcal{M}(d) \in S] \leq e^\epsilon \cdot \mathbb{P}[\mathcal{M}(d') \in S] + \delta \quad (1)$$

This definition ensures that the probability of obtaining a particular output does not change significantly when a single data point

is modified, thereby providing a formal measure of privacy protection [15]. In HPE, this definition implies that the inclusion or exclusion of a single training image, potentially representing an identifiable subject, should not significantly affect the model's predictions across downstream tasks. DP trained model ensures no particular subject's identity or appearance can be inferred from model's parameters and predictions mitigating risks such as membership inference[43] or reconstruction attacks[63].

Sensitivity and the Gaussian Mechanism: The most common method to enforce DP in an algorithm is by adding noise sampled from a Gaussian distribution. The amount of noise required is typically controlled by a parameter known as sensitivity, denoted as Δ_G , which quantifies how much the output of a function can change when a single data point is modified [29].

Definition 2: L1 Sensitivity For any function $G : \mathbb{R} \rightarrow \mathbb{R}^*$, the L1 sensitivity is the smallest value Δ_G such that for all neighboring datasets d, d' :

$$\|G(d) - G(d')\|_{L_1} \leq \Delta_G \quad (2)$$

Intuitively, sensitivity measures the maximum influence that a single data point can have on the query output. A higher sensitivity value requires adding more noise to ensure privacy. In the Gaussian mechanism, the inputs consist of the randomized algorithm \mathcal{M} , its sensitivity Δ_M , and the noise scale parameter σ . The perturbation applied to the output follows a Gaussian distribution:

$$\text{Gaussian_Mechanism}(\mathcal{M}, \Delta_M, \sigma) \triangleq \mathcal{M} + \mathcal{N}(0, \Delta_M^2 \cdot \sigma^2) \quad (3)$$

where $\mathcal{N}(0, \Delta_M^2 \cdot \sigma^2)$ represents a Gaussian distribution with mean 0 and variance $\Delta_M^2 \cdot \sigma^2$. The level of privacy protection is directly influenced by the noise scale, which is determined by σ .

Based on the analysis in [2], for any $(\epsilon, \delta) \in (0, 1)$, the Gaussian mechanism achieves (ϵ, δ) -differential privacy when:

$$\sigma = \frac{\sqrt{2 \ln(1.25/\delta)}}{\epsilon} \quad (4)$$

This formulation provides a practical approach to achieving differential privacy guarantees while controlling the trade-off between privacy and utility.

3.2 Differentially Private Stochastic Gradient Descent (DP-SGD)

A common approach to ensure DP during model training is DP-SGD, which enforces an (ϵ, δ) -DP guarantee on gradient updates [2, 9, 14]. This mechanism involves clipping gradients to a fixed threshold (C) and adding Gaussian noise calibrated based on desired privacy budget (ϵ, δ) . This process limits the influence of any single training example on the model update, thereby providing formal privacy protection [28]. The model is trained iteratively using mini-batches of input data with the SGD algorithm; this procedure is termed DP-SGD. As described in Algorithm 1, it requires an input dataset \mathcal{D} , clipping norm C and noise scale σ , which is determined by the privacy guarantee parameters (ϵ, δ) . Lower values of ϵ and δ indicates stronger privacy protection and better resistance to privacy attacks. The DP-SGD procedure in Algorithm 1 follows the standard mini-batch training approach, with the addition of lines 6, and 9, which implement gradient clipping, aggregation of the clipped gradients, and noise addition, respectively.

In our setting, we apply DP-SGD to train a TinyViT based 2D HPE model on MPII dataset. Due to the inherent structured nature of keypoint prediction task, a straight forward application of DP-SGD leads to severe degradation in performance. We empirically tune the clipping C at different rates to identify configurations that offer an effective privacy-utility tradeoff. Additionally, we employ finetuning strategy in this setting, which allows us to recover utility under strict privacy budgets[53].

Algorithm 1 DP-SGD Procedure

Input: Dataset $\mathcal{D} = \{x_1, \dots, x_n\}$, loss function \mathcal{L} , learning rate η , clipping norm C , noise scale σ , batch size B , number of iterations T

Output: Model parameters θ_T

```

1: Initialize model parameters  $\theta_0$ 
2: for  $t = 1$  to  $T$  do
3:   Sample a random mini-batch  $\mathcal{B}_t \subset \mathcal{D}$  of size  $B$ 
4:   for each  $x_i \in \mathcal{B}_t$  do
5:     Compute the gradient  $\mathbf{g}_i = \nabla_{\theta} \mathcal{L}(\theta_{t-1}, x_i)$ 
6:     Clip the gradient:  $\tilde{\mathbf{g}}_i = \mathbf{g}_i / \max\left(1, \frac{\|\mathbf{g}_i\|_2}{C}\right)$ 
7:   end for
8:   Aggregate the clipped gradients:  $\tilde{\mathbf{g}} = \frac{1}{B} \sum_{i \in \mathcal{B}_t} \tilde{\mathbf{g}}_i$ 
9:   Add noise:  $\hat{\mathbf{g}} = \tilde{\mathbf{g}} + \mathcal{N}(0, \sigma^2 C^2 \mathbf{I})$ 
10:  Update the model:  $\theta_t = \theta_{t-1} - \eta \hat{\mathbf{g}}$ 
11: end for
12: return  $\theta_T$ 

```

3.3 Gradient Subspace Identification

Our objective in this section is to improve the privacy-utility trade-off in HPE by reducing the impact of noise injection while maintaining the same privacy guarantees. The key insight driving our approach is that gradient updates during training tend to concentrate within a low-dimensional subspace rather than utilizing the full parameter space. By identifying and projecting noisy gradients onto this informative subspace, we filter out less relevant directions. In this way, we preserve the signal quality of gradient updates while adhering to DP constraints [62], and removing privacy-sensitive information that is not strictly required to minimize the loss, such as facial features. To estimate the intrinsic structure of the gradient space, we employ a small auxiliary public dataset S_{pub} , which is drawn from a similar distribution as that of private training set. This subset is used to estimate the principal subspace of the gradient covariance. Given the model parameters $\mathbf{w} \in \mathbb{R}^p$, the second moment matrix of gradients over S_{pub} is calculated as:

$$M(\mathbf{w}) = \frac{1}{m} \sum_{i=1}^m \nabla l(\mathbf{w}, \tilde{z}_i) \nabla l(\mathbf{w}, \tilde{z}_i)^T \quad (5)$$

where m denotes the number of public samples and \tilde{z}_i represents an input sample from S_{pub} . The eigenvectors corresponding to the top k eigenvalues are stacked to form the projection matrix $\hat{\mathbf{V}} \in \mathbb{R}^{p \times k}$ which forms the low-dimensional approximation of the full gradient space; this maps the p -dimensional gradients to a smaller k -dimensional subspace. This projection matrix is updated periodically to accommodate changes in gradient distributions over the training period.

In the DP-SGD setup, for each mini-batch sampled from the private dataset S_{priv} , per-sample gradients are computed and the sensitivity of each individual gradient is bounded by the clipping threshold C :

$$\tilde{g}_i = \text{clip}(\nabla l(\mathbf{w}, z_i), C) \quad (6)$$

The clipped gradients are aggregated over the batch and Gaussian noise is added to ensure differential privacy

$$g = \frac{1}{B} \sum_{i \in B} \tilde{g}_i + \mathcal{N}(0, \sigma^2 C^2 \mathbf{I}), \quad (7)$$

where B is the size of the mini-batch and σ is the standard deviation. The full noisy gradient g is then projected on to the estimated low-dimensional subspace as

$$g_{proj} = (\hat{\mathbf{V}} \hat{\mathbf{V}}^T) g \quad (8)$$

This restricts the update direction to the subspace where the gradients exhibit the highest variance, thereby filtering out noise components residing in less informative directions. The model parameters are then updated using the projected gradient. Since the projection is applied as a post-processing step after noise addition, the overall DP guarantee remains intact.

3.4 Lightweight 2D-HPE: Integrating TinyViT Backbone with Coordinate Classification

For our 2D-HPE models, we adopt TinyViT [49] as the backbone. It is a small sized four-stage efficient hierarchical vision transformer which is well suited for resource-constrained vision tasks. The model adopts a multi-stage architecture where in the spatial resolution is progressively reduced and the feature representation expands. TinyViT follows a hybrid architectural design containing convolutional layers at the initial stages followed by self-attention mechanisms. Unlike standard ViT models, TinyViT employs a two-layer convolutional embedding. In the first stage of the network, it employs MBConv [24] blocks from MobileNetV2 to efficiently learn the low-level representation. The last three stages consists of transformer blocks hierarchically. Each stage consists of multi-head-self-attention (MHSA) layers, feed forward network (FFN) and 3×3 depthwise convolutions between the MHSA and FFN layers.

For keypoint localization, we augment the TinyViT backbone model with a coordinate classification output stage [32]. Given an input image $I \in \mathbb{R}^{C \times H \times W}$ and a ground truth keypoint $p_i = (x_i, y_i)$ for the i^{th} joint, the continuous coordinates are quantized into discrete bins via a splitting factor $k \geq 1$. Formally, the quantized coordinates are computed as:

$$p'_i = (\lfloor x_i \cdot k \rfloor, \lfloor y_i \cdot k \rfloor),$$

where $\lfloor \cdot \rfloor$ denotes the rounding operation. This binning reduces quantization error while preserving high localization precision.

Within our network, the convolutional head produces a 16-channel feature map, with each channel corresponding to a specific joint. These joint-specific features are upsampled and flattened to form a compact representation used for classification over the discrete coordinate bins. To improve robustness, we employ Gaussian label smoothing on the classification targets. This smoothing accounts for spatial correlations by assigning soft labels that reflect the relevance of neighboring bins. Finally, the discrete classification

outputs are decoded back into continuous coordinates to yield the final keypoint predictions.

4 Experiments

4.1 Datasets and Evaluation Design

In our experiments, we evaluated our framework on two widely used human pose datasets: MS COCO Keypoint Dataset [35] and MPII dataset [5]. Our methodology assumes that the COCO dataset serves as a public dataset used for pre-training the network weights, while MPII functions as a private dataset on which we apply the differential privacy techniques.

Specifically, our models are pretrained on the COCO *train2017* set, which consists of approximately 118k images with around 140k annotated human instances, each with 17 joint annotations. The *val2017* set consisting of around 5k images is used for validation. For evaluating the trade-off between utility and performance under various DP-SGD techniques we employ the MPII Human Pose Dataset consisting of 40k human instances, each labeled with 16 joint annotations. When transferring the model from COCO to MPII, we adjust for the keypoint discrepancy between datasets. We employ the Percentage of Correct Keypoints normalized by head (PCKh) [5] as an evaluation metric.

Our experimental framework explores three distinct DP training scenarios: Fine-Tuning with frozen backbone, Full Fine-Tuning and, Training from scratch. For the first scenario, we specifically freeze the first three stages of the backbone and finetune the fourth stage and all instances of layer norm[11]. All models are trained under differential privacy constraints using DP-SGD with various clipping norms and privacy budgets (ϵ). Each model undergoes training for a total of 25 epochs, as we empirically observed no significant performance improvements when extending training beyond this duration under DP constraints. Throughout all experiments, we maintain a fixed input resolution of 256×192 pixels to ensure consistency across experiments and enable comparison with prior work.

For the privacy parameter settings, we use three gradient clipping norms $C = \{1.0, 0.1, 0.01\}$, with target privacy budgets of $\epsilon = \{0.2, 0.4, 0.6, 0.8, 1.0, 3.0, 5.0, 7.0\}$, which range from tight privacy budgets to more relaxed. We adopt Renyi Differential Privacy (RDP) [39] for privacy accounting with the privacy parameter $\delta = 4\epsilon - 5$.

For the projection method, we randomly select 100 samples from the training dataset of MPII as S_{pub} (ensuring no image overlap with the private data) with the remaining data forming the private training set S_{priv} . The default projection dimension K is set to 50 for all experiments.

4.2 Results

4.2.1 Baseline Results: Non-Private. Table 1 presents non-private baseline results from our model on the MPII dataset under three different training strategies: i) finetuning ii) finetuning from scratch and iii) training from scratch. These results demonstrate high pose estimation accuracy, representing best case performances in absence of DP noise.

Table 1: MPII Results: Non-Private Baselines for our HPE model on the MPII dataset

Training Strategy	Head	Shoulder	Elbow	Wrist	Hip	Knee	Ankle	Mean	Mean@0.1
Finetuning	97.07	95.86	89.59	83.61	89.29	85.31	81.48	89.36	31.33
Finetuning from scratch	96.45	95.84	88.07	82.18	88.78	83.01	79.45	88.28	28.11
Training from scratch	93.89	89.32	75.34	65.24	80.04	66.15	60.60	76.89	17.26

4.2.2 Baseline Results with DP-SGD. Table 2 presents detailed performance results on the MPII dataset under the mentioned training strategies. The evaluation is carried out across multiple settings with different levels of privacy parameters ϵ and clipping thresholds C , and training strategies.

For standard finetuning with DP-SGD, we observe that lower clipping thresholds consistently result in better PCKh@0.5 scores across all joints. Specifically, with a clipping threshold of $C = 0.01$, results substantially outperforms other thresholds, demonstrating that tighter gradient clipping significantly benefits model performance under strict privacy budgets. Notably, at $\epsilon = 0.2$, mean PCKh@0.5 with $C = 0.01$ reaches 63.85%, outperforming the 28.46% achieved with $C = 0.1$ and the mere 5.94% with $C = 1.0$. As expected, performance improves monotonically as ϵ increases across all joints and mean accuracy metrics. At a relaxed privacy constraint of $\epsilon = 7.0$, PCKh@0.5 with the optimal clipping threshold ($C = 0.01$) achieves 82.15%, highlighting the practical effectiveness of fine-tuning with a low clipping threshold for DP-SGD in pose estimation tasks.

In the scenario of fine-tuning from scratch, the overall performance noticeably deteriorates compared to standard fine-tuning. Under tight privacy constraints (e.g., $\epsilon = 0.2$), performance is considerably limited across all clipping thresholds, with mean accuracy at $C = 0.01$ dropping to 24.05%. Although, we observe similar patterns of improved accuracy values with larger ϵ and tighter clipping thresholds, the best performance in the settings ($\epsilon = 7.0$, $C = 0.01$) reaches only 55.66%, substantially lower than standard fine-tuning.

Training entirely from scratch presents the most significant challenge, with DP-SGD struggling to achieve competitive performance across all configurations. This demonstrates the inherent challenge of training deep neural networks privately without leveraging pre-trained knowledge. Accuracy metrics across most body joints remain very low, rarely exceeding 20%, even at a weaker privacy constraints (say, $\epsilon = 7.0$). The highest overall mean accuracy in this setting is a mere 17.37% at ($C = 0.01$, $\epsilon = 7.0$), underscoring the difficulty of privacy-preserving training with random initialization.

Overall, these results clearly indicate that fine-tuning pretrained models with small gradient clipping thresholds effectively reduces the performance degradation imposed by DP. Meanwhile, training from scratch remains remarkably challenging, even with careful DP-SGD configuration.

4.2.3 Improved Results via Projection. Table 3 presents results on the MPII dataset for HPE using DP-SGD enhanced with the projection-based approach. Our experiments maintain fair training strategies and privacy parameters for direct comparison with baseline methods under DP-SGD in table 2.

In the fine-tuning scenario, we observe substantial improvements compared to approaches without projection. Even under stringent

Table 2: MPII Results: DP-SGD.

Privacy Parameter(ϵ)	Head	Shoulder	Elbow	Wrist	Hip	Knee	Ankle	Mean	Mean@0.1
Finetuning									
C = 1.0									
$\epsilon = 0.2$	0.00	5.15	13.31	6.00	10.20	2.18	0.21	5.94	0.29
$\epsilon = 0.4$	0.99	6.27	14.83	7.68	12.97	2.38	3.26	8.36	0.34
$\epsilon = 0.6$	0.31	13.06	21.56	8.43	19.16	3.00	3.59	12.19	0.58
$\epsilon = 0.8$	2.97	10.43	19.16	7.06	22.31	3.75	8.12	12.53	0.61
$\epsilon = 1.0$	2.46	14.52	19.35	7.40	28.84	3.69	5.64	14.36	0.72
$\epsilon = 3.0$	10.54	18.19	23.59	8.48	29.83	6.85	11.27	18.74	0.95
$\epsilon = 5.0$	10.95	23.91	29.07	9.61	29.41	6.97	12.68	20.42	1.01
$\epsilon = 7.0$	15.76	21.23	29.03	10.18	34.69	10.24	10.84	22.26	1.18
C = 0.1									
$\epsilon = 0.2$	30.73	35.51	31.19	13.43	37.96	12.59	13.30	28.46	1.61
$\epsilon = 0.4$	43.01	49.92	47.98	20.20	50.67	18.22	21.56	39.78	2.43
$\epsilon = 0.6$	53.10	59.51	52.00	24.55	58.54	22.65	22.65	45.18	2.86
$\epsilon = 0.8$	64.56	64.44	53.09	28.29	60.05	30.29	28.74	49.93	3.42
$\epsilon = 1.0$	64.22	65.59	53.93	30.41	62.77	32.60	28.25	51.26	3.66
$\epsilon = 3.0$	74.90	77.14	65.91	48.12	65.36	39.61	38.07	60.82	4.89
$\epsilon = 5.0$	77.83	78.92	64.92	44.25	68.32	47.59	37.32	62.09	5.17
$\epsilon = 7.0$	78.34	80.42	69.80	47.13	68.24	48.16	38.24	63.83	5.70
C = 0.01									
$\epsilon = 0.2$	78.14	83.36	65.21	47.49	69.98	47.35	39.02	63.85	5.68
$\epsilon = 0.4$	83.83	88.88	77.02	63.83	74.87	62.50	52.12	73.77	9.30
$\epsilon = 0.6$	87.11	90.05	78.71	70.05	75.37	66.61	59.42	76.85	11.05
$\epsilon = 0.8$	87.79	90.32	78.95	71.99	77.91	69.07	61.55	78.17	11.91
$\epsilon = 1.0$	88.54	91.47	80.43	71.70	77.95	69.39	60.34	78.55	12.36
$\epsilon = 3.0$	91.47	92.58	81.69	74.81	79.80	72.15	66.46	80.97	15.56
$\epsilon = 5.0$	92.26	93.29	83.38	75.16	81.34	74.15	67.93	82.11	16.26
$\epsilon = 7.0$	91.85	93.16	82.60	75.79	82.74	73.87	67.15	82.15	16.47
Finetuning from scratch									
C = 1.0									
$\epsilon = 0.2$	4.09	2.96	0.82	1.51	0.71	0.75	0.59	1.39	0.06
$\epsilon = 0.4$	6.51	7.51	3.44	3.67	1.66	1.04	1.06	5.95	0.22
$\epsilon = 0.6$	16.17	11.79	7.41	3.92	9.23	9.27	1.82	8.67	0.37
$\epsilon = 0.8$	8.94	17.05	8.40	3.79	10.04	8.38	2.95	9.34	0.39
$\epsilon = 1.0$	9.55	11.48	8.54	4.83	4.17	10.16	3.33	8.05	0.32
$\epsilon = 3.0$	7.13	13.09	11.68	11.27	17.17	11.32	7.68	12.21	0.50
$\epsilon = 5.0$	6.04	14.67	10.76	5.11	21.86	11.42	7.96	11.97	0.51
$\epsilon = 7.0$	10.20	17.90	12.99	8.77	20.89	10.72	9.57	13.68	0.63
C = 0.1									
$\epsilon = 0.2$	12.48	20.87	15.70	10.91	23.39	13.96	8.36	16.11	0.68
$\epsilon = 0.4$	16.68	22.69	21.15	11.10	24.10	12.98	9.38	18.64	0.80
$\epsilon = 0.6$	23.26	28.07	21.70	13.06	26.92	14.57	9.73	21.73	1.07
$\epsilon = 0.8$	28.58	29.14	21.36	13.18	27.40	14.31	9.09	22.74	1.10
$\epsilon = 1.0$	33.42	28.67	20.59	11.75	27.33	14.83	10.51	22.61	1.18
$\epsilon = 3.0$	45.09	35.72	25.53	14.53	30.92	15.96	13.46	27.68	1.47
$\epsilon = 5.0$	50.17	42.46	25.96	15.00	33.77	17.41	14.97	30.74	1.69
$\epsilon = 7.0$	55.42	40.17	27.53	15.81	34.88	17.75	17.29	32.21	1.89
C = 0.01									
$\epsilon = 0.2$	28.89	31.52	22.43	12.11	27.37	16.72	10.39	24.05	1.16
$\epsilon = 0.4$	49.25	43.19	26.28	15.01	33.58	18.05	15.28	30.94	1.86
$\epsilon = 0.6$	60.20	50.68	30.99	16.99	37.84	20.15	20.34	35.77	2.25
$\epsilon = 0.8$	62.28	54.33	36.48	21.66	43.36	22.43	21.42	39.86	2.86
$\epsilon = 1.0$	66.68	57.83	37.14	22.49	43.41	23.92	22.48	41.26	2.97
$\epsilon = 3.0$	74.86	68.65	47.37	29.16	52.93	32.66	30.51	49.95	4.29
$\epsilon = 5.0$	77.83	71.62	51.37	33.40	56.19	37.72	34.65	53.65	4.97
$\epsilon = 7.0$	78.79	72.84	54.01	37.49	57.33	39.17	37.22	55.66	5.41
Training from scratch									
C = 1.0									
$\epsilon = 0.2$	0.14	0.05	0.37	0.02	0.64	0.26	0.35	0.30	0.02
$\epsilon = 0.4$	1.71	0.07	0.07	0.15	0.28	3.28	0.02	0.68	0.03
$\epsilon = 0.6$	0.03	4.64	0.00	1.25	0.90	3.10	0.05	1.45	0.07
$\epsilon = 0.8$	0.31	0.00	1.76	0.26	0.00	0.00	0.90	0.44	0.02
$\epsilon = 1.0$	0.03	0.07	2.15	0.51	1.06	0.77	0.00	0.71	0.03
$\epsilon = 3.0$	0.51	0.03	1.67	0.02	2.75	0.52	2.20	1.05	0.04
$\epsilon = 5.0$	0.20	5.33	0.22	0.33	1.13	0.77	1.65	1.37	0.04
$\epsilon = 7.0$	0.20	0.07	0.82	8.62	0.16	1.29	0.07	1.66	0.08
C = 0.1									
$\epsilon = 0.2$	1.09	0.03	2.97	7.01	1.28	1.23	0.50	2.33	0.09
$\epsilon = 0.4$	0.14	5.04	6.49	4.69	18.87	0.67	0.24	5.84	0.23
$\epsilon = 0.6$	0.10	9.51	8.01	9.58	22.90	2.08	1.23	8.12	0.33
$\epsilon = 0.8$	0.24	8.07	5.25	9.46	17.03	2.04	2.39	6.85	0.28
$\epsilon = 1.0$	0.24	13.33	14.57	10.26	23.65	2.86	1.87	10.63	0.36
$\epsilon = 3.0$	0.41	15.08	11.83	9.37	20.10	3.63	1.18	9.54	0.37
$\epsilon = 5.0$	1.06	19.51	9.56	10.35	15.77	3.89	1.44	10.34	0.44
$\epsilon = 7.0$	1.19	10.80	7.81	8.72	23.80	4.15	0.85	9.16	0.36
C = 0.01									
$\epsilon = 0.2$	0.31	10.31	10.07	4.90	13.33	3.41	1.77	8.17	0.36
$\epsilon = 0.4$	1.33	15.61	9.17	8.96	19.92	3.87	1.32	10.13	0.48
$\epsilon = 0.6$	6.79	17.24	13.50	9.60	21.53	5.74	2.13	12.68	0.56
$\epsilon = 0.8$	13.27	16.76	13.38	9.68	19.87	5.48	2.17	12.74	0.54
$\epsilon = 1.0$	9.41	22.72	14.61	11.21	23.89	14.43	3.35	16.12	0.70
$\epsilon = 3.0$	9.79	19.92	16.82	11.43	22.61	15.19	4.09	15.99	0.72
$\epsilon = 5.0$	10.44	19.89	16.84	11.16	24.42	12.81	4.23	16.09	0.75
$\epsilon = 7.0$	15.04	22.06	17.27	11.82	23.63	14.27	6.92	17.37	0.78

privacy budgets (low ϵ values), our method achieves high accuracy, particularly with lower clipping thresholds ($C = 0.01$). For instance, at the strictest privacy budget ($\epsilon = 0.2$) and the lowest clipping threshold ($C = 0.01$), the mean accuracy reaches 78.48%, significantly outperforming both higher clipping thresholds (73.13% at

$C = 0.1$) and far exceeding the 10.34% at $C = 1.0$. As privacy constraints become higher, performance improves consistently across all joints, with peak performance of 80.98% mean accuracy observed at $\epsilon = 7.0$ and $C = 0.01$. Notably, at moderate privacy budgets ($\epsilon = 0.8$), we observe substantial accuracy gains for traditionally challenging joints to extract such as wrists and ankles.

In the setting of fine-tuning from scratch with DP projection, overall accuracies are markedly lower compared to freezing earlier layers. However, our proposed method still significantly outperforms corresponding results from the standard DP-SGD method without projection. Under strict privacy budgets (e.g., $\epsilon = 0.2$), mean accuracy is limited, achieving a maximum of 53.54% at $C = 0.01$. Performance improves progressively with relaxed privacy constraints, reaching up to 69.81% accuracy at $\epsilon = 7.0$ and $C = 0.01$. The noticeable performance fluctuations at intermediate settings highlight the inherent sensitivity to both privacy budgets and clipping thresholds when fine-tuning from scratch.

For training entirely from scratch, limitations remain pronounced despite improvements over standard DP-SGD. Accuracies remain relatively low across all clipping thresholds and privacy budgets, though slightly outperforming standard DP-SGD without projection. Even at relaxed privacy budgets ($\epsilon = 7.0$), the highest mean accuracy achieved is only 14.89% at $C = 0.01$. These results highlight the fundamental challenge of fully private training without leveraging pretrained knowledge, even when employing gradient projection techniques.

Overall, our results presented in Table 3 strongly suggest that incorporating DP-SGD with projection significantly improves model performance, particularly when combined with strategic fine-tuning (freezing layers) and careful selection of gradient clipping thresholds. Among all evaluated approaches, fine-tuning with frozen initial layers at a low clipping threshold ($C = 0.01$) emerges as the most effective strategy, achieving an excellent balance between model accuracy and privacy protection.

Figure 1 compares the mean accuracy improvements achieved by introducing projection to standard DP-SGD across broad range of privacy budgets and clipping thresholds.

The integration of gradient projection in DP-SGD consistently boosts performance across nearly all experimental configurations, demonstrating its effectiveness in enhancing differential private 2D-HPE training. These improvements are most substantial at tight privacy budgets (lower ϵ values), where projection significantly mitigates the inherent accuracy-privacy trade-off typically observed in DP training. We observe a particularly strong impact of projection with higher clipping thresholds (e.g., $C = 1.0$ and $C = 0.1$). Here, projection dramatically boost performance under stringent privacy constraints. For example, at $\epsilon = 0.4$ and $C = 1.0$ accuracy increases more than 25% (from 8.36% to 36.99%), highlighting the significant advantage gained by incorporating projection under challenging privacy settings.

The benefits of projection become less pronounced at the lowest clipping threshold ($C = 0.01$) and more relaxed privacy budgets (higher ϵ values). In these cases, while projection still achieves improved accuracy, the gains plateau, suggesting that extremely tight gradient clipping already constraints gradients efficiently in low privacy settings. Interestingly, projection proves especially beneficial when fine-tuning from scratch with $C = 0.01$, substantially

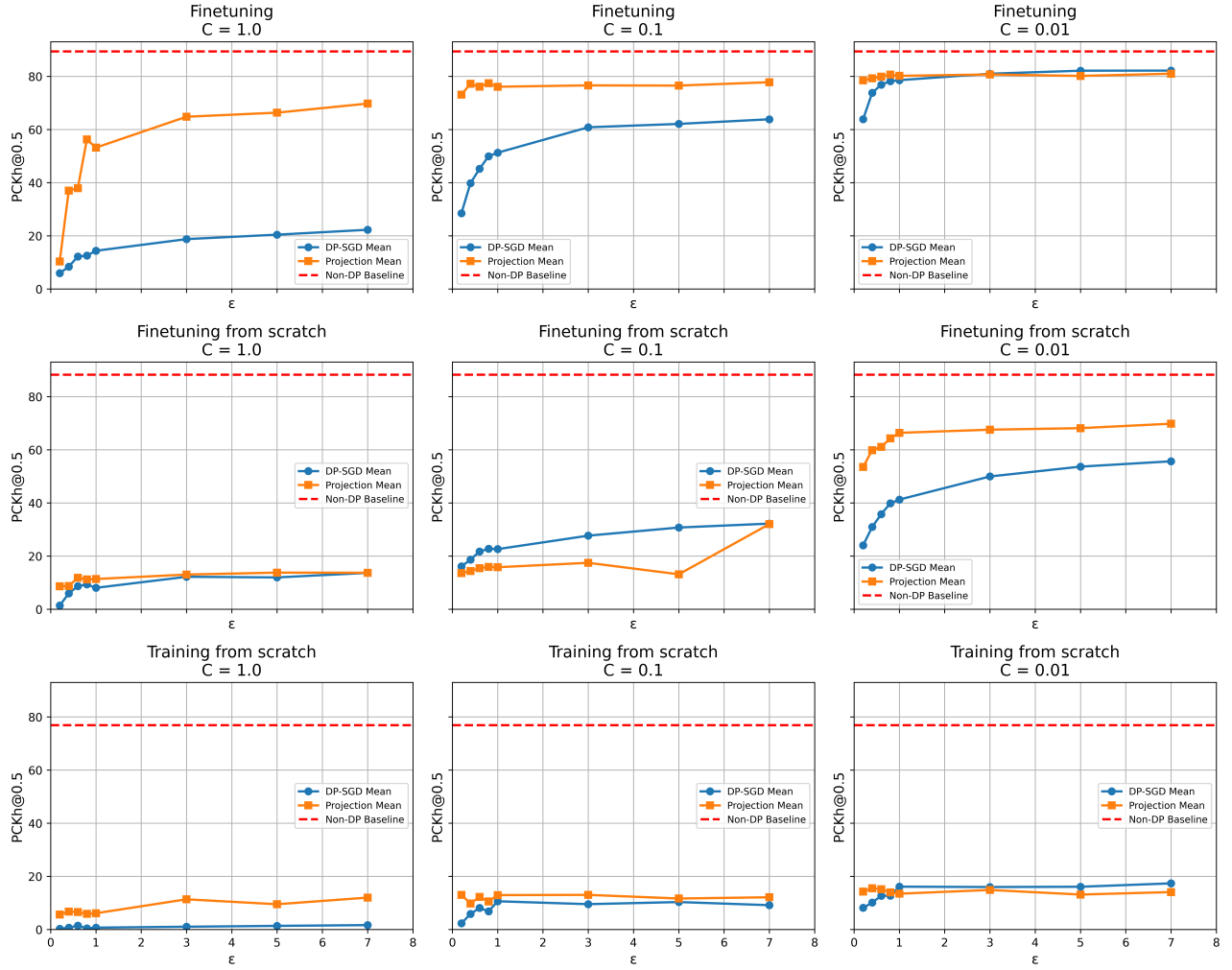


Figure 1: Comparison of PCKh@0.5 with and without projection across different training strategies with varied epsilons and clipping norm.

narrowing the performance gap typically observed compared to fine-tuning from pretrained models. Conversely, projection’s benefit are observed only at low *epsilon* values when training entirely from scratch with $C = 0.01$. These results might indicate how challenging it is to train DP models from scratch.

In summary, our projection-enhanced DP-SGD approach for 2D-HPE consistently improves accuracy under DP constraints, with the greatest benefits emerging under stricter privacy conditions and moderate gradient clipping thresholds. These findings provide valuable guidance for applying DP in HPE and other sensitive computer vision, deep learning tasks.

5 Conclusion

Our work presents the first differentially private (DP) approach to 2D human pose estimation (HPE), addressing critical privacy concerns while maintaining utility for multimedia applications. By integrating Projected DP-SGD (PDP-SGD) and adapting TinyViT with

a coordinate classification head, we achieved remarkable accuracy (78.48% PCKh@0.5 at *epsilon* = 0.2) even under strict privacy constraints, significantly outperforming standard DP-SGD procedure. Our comprehensive experiments on the MPII dataset revealed that fine-tuning with frozen initial layers and a low clipping threshold ($C=0.01$) provides the optimal balance between privacy and performance, with notable improvements for challenging joints. Unlike traditional anonymization techniques that compromise data utility, our method maintains analytical value while providing formal privacy guarantees, laying a solid foundation for privacy-preserving HPE in sensitive domains such as healthcare and activity recognition. This work demonstrates that DP pose estimation is not only feasible but can approach non-private performance levels while ensuring strong privacy protection.

Acknowledgments

The quick brown fox jumps over the lazy dog

Table 3: MPII Results: DP-SGD with Projection.

Privacy Parameter(ϵ)	Head	Shoulder	Elbow	Wrist	Hip	Knee	Ankle	Mean	Mean@0.1
Finetuning									
C = 1.0									
$\epsilon = 0.2$	3.48	14.79	6.85	8.38	17.36	8.85	8.62	10.34	0.42
$\epsilon = 0.4$	54.67	55.45	32.54	23.70	37.23	21.44	13.30	36.99	2.33
$\epsilon = 0.6$	55.97	49.10	31.99	28.22	39.67	24.10	14.34	37.90	2.31
$\epsilon = 0.8$	71.18	76.19	55.51	46.60	53.97	39.13	32.97	56.26	4.19
$\epsilon = 1.0$	71.62	75.61	46.67	39.32	58.73	34.70	24.19	53.17	3.73
$\epsilon = 3.0$	81.48	83.53	70.46	64.98	46.24	53.90	39.11	64.79	7.09
$\epsilon = 5.0$	78.31	82.59	72.76	65.14	50.32	56.50	44.43	66.32	7.05
$\epsilon = 7.0$	72.51	87.64	73.85	65.10	61.55	59.14	53.19	69.74	7.66
C = 0.1									
$\epsilon = 0.2$	88.85	89.44	75.78	68.46	61.21	63.83	54.68	73.13	10.56
$\epsilon = 0.4$	88.44	89.84	78.92	72.62	70.21	69.45	61.08	77.17	12.55
$\epsilon = 0.6$	90.31	90.20	79.27	71.43	66.02	68.75	58.01	76.11	12.21
$\epsilon = 0.8$	91.51	90.39	79.51	72.84	71.23	67.86	59.78	77.41	12.88
$\epsilon = 1.0$	90.42	89.23	79.50	68.39	66.52	68.83	61.64	76.07	11.20
$\epsilon = 3.0$	89.73	90.13	78.75	71.25	70.33	66.19	60.65	76.59	12.22
$\epsilon = 5.0$	90.79	89.76	75.10	70.59	71.94	67.40	61.95	76.51	12.23
$\epsilon = 7.0$	92.05	91.59	77.81	72.95	70.07	69.67	62.37	77.78	12.53
C = 0.01									
$\epsilon = 0.2$	92.02	90.78	79.10	72.47	72.72	70.74	64.29	78.48	13.67
$\epsilon = 0.4$	91.81	90.74	79.92	72.04	75.42	71.79	65.78	79.23	13.49
$\epsilon = 0.6$	92.29	91.78	80.48	73.75	74.16	72.29	67.88	79.89	14.28
$\epsilon = 0.8$	92.29	91.49	80.86	74.52	75.32	73.91	69.77	80.63	14.61
$\epsilon = 1.0$	93.21	91.36	80.11	73.70	77.55	71.61	66.93	80.17	14.76
$\epsilon = 3.0$	92.70	92.10	79.85	74.80	76.61	73.81	68.40	80.70	14.77
$\epsilon = 5.0$	91.58	91.12	80.33	73.62	76.42	73.36	67.76	80.14	13.86
$\epsilon = 7.0$	91.81	92.58	81.78	75.45	75.30	73.77	69.37	80.98	14.65
Finetuning from scratch									
C = 1.0									
$\epsilon = 0.2$	0.48	8.93	8.86	8.24	20.72	3.77	1.75	8.64	0.31
$\epsilon = 0.4$	4.13	14.88	14.32	6.99	3.41	5.80	3.73	8.74	0.38
$\epsilon = 0.6$	3.48	16.34	9.90	12.35	13.21	13.48	10.23	11.85	0.56
$\epsilon = 0.8$	2.69	15.73	11.20	11.79	19.65	6.83	1.94	11.22	0.51
$\epsilon = 1.0$	3.99	16.34	8.54	9.20	15.75	10.05	7.53	11.37	0.40
$\epsilon = 3.0$	8.39	16.98	11.56	10.74	18.71	10.88	5.79	13.05	0.60
$\epsilon = 5.0$	15.42	18.19	10.12	7.99	24.48	12.39	1.65	13.77	0.52
$\epsilon = 7.0$	10.88	15.47	9.12	10.81	21.78	12.05	7.89	13.72	0.64
C = 0.1									
$\epsilon = 0.2$	4.40	18.99	16.99	9.42	18.07	10.70	6.78	13.58	0.63
$\epsilon = 0.4$	12.45	15.30	17.25	10.90	21.50	9.61	7.01	14.36	0.61
$\epsilon = 0.6$	15.59	15.64	16.70	10.50	19.49	14.19	7.98	15.43	0.66
$\epsilon = 0.8$	13.34	23.30	15.51	10.08	20.06	8.68	9.05	15.92	0.61
$\epsilon = 1.0$	10.54	20.67	15.08	11.36	22.69	8.46	8.48	15.80	0.65
$\epsilon = 3.0$	17.33	23.27	17.66	11.94	21.38	10.80	9.21	17.47	0.75
$\epsilon = 5.0$	2.97	16.54	7.26	9.63	21.46	15.74	5.98	13.14	0.56
$\epsilon = 7.0$	36.22	48.30	29.37	20.73	33.36	17.31	9.49	32.03	1.81
C = 0.01									
$\epsilon = 0.2$	82.44	69.58	49.75	43.23	43.31	39.11	36.56	53.54	5.87
$\epsilon = 0.4$	83.77	75.70	55.19	50.44	52.12	46.12	45.35	59.82	7.87
$\epsilon = 0.6$	86.02	74.25	61.31	52.96	51.39	46.75	45.42	61.09	8.61
$\epsilon = 0.8$	87.14	77.77	63.32	56.18	57.14	50.92	48.89	64.28	9.68
$\epsilon = 1.0$	88.17	81.13	66.54	56.66	61.78	51.86	48.54	66.37	9.92
$\epsilon = 3.0$	88.27	81.98	67.09	57.41	61.76	54.93	52.43	67.55	10.23
$\epsilon = 5.0$	90.14	82.88	66.35	57.29	64.24	55.25	52.43	68.13	10.33
$\epsilon = 7.0$	91.00	83.34	69.20	60.22	64.67	57.14	55.01	69.81	11.31
Training from scratch									
C = 1.0									
$\epsilon = 0.2$	0.07	1.77	10.07	11.07	12.74	1.37	0.02	5.65	0.26
$\epsilon = 0.4$	1.36	6.98	17.69	9.77	5.24	0.95	0.07	6.76	0.28
$\epsilon = 0.6$	0.07	1.00	14.47	12.44	6.42	7.19	1.87	6.57	0.31
$\epsilon = 0.8$	0.17	7.24	11.71	5.91	2.68	4.27	1.23	5.89	0.24
$\epsilon = 1.0$	0.14	1.39	6.51	8.94	18.78	2.96	2.01	6.12	0.29
$\epsilon = 3.0$	0.38	13.79	12.48	9.53	24.72	8.26	2.34	11.37	0.51
$\epsilon = 5.0$	1.47	10.70	9.77	7.56	22.04	3.41	0.92	9.51	0.39
$\epsilon = 7.0$	0.78	12.55	13.21	10.62	23.18	8.76	2.39	12.01	0.47
C = 0.1									
$\epsilon = 0.2$	1.19	18.05	12.78	9.53	22.66	7.64	5.95	13.05	0.56
$\epsilon = 0.4$	0.75	13.08	6.17	5.55	21.91	3.36	5.50	9.80	0.41
$\epsilon = 0.6$	1.98	21.28	8.16	11.05	19.70	4.11	4.72	12.24	0.56
$\epsilon = 0.8$	1.30	13.20	4.48	8.31	22.62	6.73	4.27	10.57	0.43
$\epsilon = 1.0$	2.66	17.26	8.47	7.50	22.57	15.53	3.59	12.96	0.62
$\epsilon = 3.0$	3.75	15.20	15.17	11.67	22.00	4.69	5.67	13.04	0.55
$\epsilon = 5.0$	0.65	12.31	9.14	10.49	23.99	9.29	4.56	11.67	0.46
$\epsilon = 7.0$	1.13	14.74	6.90	10.71	22.54	7.19	9.49	12.14	0.51
C = 0.01									
$\epsilon = 0.2$	5.15	15.10	15.07	12.39	19.61	10.28	8.83	14.26	0.65
$\epsilon = 0.4$	9.21	20.60	15.78	10.67	22.33	13.06	7.01	15.54	0.70
$\epsilon = 0.6$	17.09	19.70	6.89	10.50	22.36	15.88	10.51	15.15	0.62
$\epsilon = 0.8$	9.48	19.55	16.12	10.91	22.45	6.61	3.57	13.96	0.60
$\epsilon = 1.0$	4.40	19.75	8.40	10.59	22.54	10.92	6.90	13.48	0.59
$\epsilon = 3.0$	15.45	21.79	8.23	10.57	23.21	12.59	4.65	14.89	0.66
$\epsilon = 5.0$	15.93	14.83	6.34	9.90	23.11	12.33	7.25	13.16	0.59
$\epsilon = 7.0$	0.75	17.02	14.79	9.39	23.58	15.76	4.91	14.09	0.55

References

- [n. d.]. Ethical issues in using ambient intelligence in health-care settings, author=Nicole Martinez-Martin, Zelun Luo, Amit Kaushal, Ehsan Adeli, Albert Haque, Sara S Kelly, Sarah Wieten, Mildred K Cho, David Magnus, Li Fei-Fei, Kevin Schulman, Arnold Milstein, journal=The Lancet Digital Health, year=2021. ([n. d.]).
- Martin Abadi, Andy Chu, Ian Goodfellow, H Brendan McMahan, Ilya Mironov, Kunal Talwar, and Li Zhang. 2016. Deep Learning with Differential Privacy. In *Proceedings of the 2016 ACM SIGSAC Conference on Computer and Communications Security*. ACM, 308–318. doi:10.1145/2976749.2978318
- Wisam Abbasi, Paolo Mori, and Andrea Saracino. 2025. Trading-Off Privacy, Utility, and Explainability in Deep Learning-Based Image Data Analysis. *IEEE Transactions on Dependable and Secure Computing* 22, 01 (Jan. 2025), 388–405. doi:10.1109/TDSC.2024.3400608
- Shafiq Ahmad, Pietro Morerio, and Alessio Del Bue. 2024. Event anonymization: privacy-preserving person re-identification and pose estimation in event-based vision. *IEEE Access* (2024).
- Mykhaylo Andriluka, Leonid Pishchulin, Peter Gehler, and Bernt Schiele. 2014. 2d human pose estimation: New benchmark and state of the art analysis. In *Proceedings of the IEEE Conference on computer Vision and Pattern Recognition*. 3686–3693.
- Bruno Artacho and Andreas Savakis. 2020. Unipose: Unified human pose estimation in single images and videos. In *Proceedings of the IEEE/CVF conference on computer vision and pattern recognition*. 7035–7044.
- Simone Barattin, Christos Tzelepis, Ioannis Patras, and Nicu Sebe. 2023. Attribute-preserving face dataset anonymization via latent code optimization. In *Proceedings of the IEEE/CVF conference on computer vision and pattern recognition*. 8001–8010.
- Fani Deligianni Bhargav Sivangi. 2024. Knowledge Distillation with Global Filters for Efficient Human Pose Estimation. In *British Machine Vision Conference (BMVC)*.
- Franziska Boenisch, Antoni Kowalczyk, Jan Dubinski, Atiyeh Ashari Ghomi, Yi Sui, George Stein, Jiapeng Wu, Jesse C Cresswell, and Adam Dziedzic. 2024. Benchmarking Robust Self-Supervised Learning Across Diverse Downstream Tasks. *CoRR* abs/2407.12588 (2024). <https://dblp.org/rec/journals/corr/abs-2407-12588.html>
- Rohit Kumar Bondugula, Siba K Udgata, and Kaushik Bhargav Sivangi. 2023. A novel deep learning architecture and MINIROCKET feature extraction method for human activity recognition using ECG, PPG and inertial sensor dataset. *Applied Intelligence* 53, 11 (2023), 14400–14425.
- Soham De, Leonard Berrada, Jamie Hayes, Samuel L Smith, and Borja Balle. 2022. Unlocking high-accuracy differentially private image classification through scale. *arXiv preprint arXiv:2204.13650* (2022).
- Bappaditya Debnath, Mary O'brien, Motonori Yamaguchi, and Ardhendu Behera. 2018. Adapting MobileNets for mobile based upper body pose estimation. In *2018 15th IEEE International Conference on Advanced Video and Signal Based Surveillance (AVSS)*. IEEE, 1–6.
- Fani Deligianni, Yao Guo, and Guang-Zhong Yang. 2019. From emotions to mood disorders: A survey on gait analysis methodology. *IEEE journal of biomedical and health informatics* 23, 6 (2019), 2302–2316.
- Lionel Dupuy, Sergio Yovine, Federico Pan, Nicolas Basset, and Thao Dang. 2022. Towards Efficient Active Learning of PDFAs. In *Proceedings of the 2022 International Conference on Learning Representations*. ICLR. <https://arxiv.org/abs/2206.09004>
- Cynthia Dwork. 2021. The promise of differential privacy: a tutorial on algorithmic techniques. In *2011 IEEE 52nd Annual Symposium on Foundations of Computer Science, D (Oct. 2011)*. Citeseer, 1–2.
- Cynthia Dwork, Frank McSherry, Kobbi Nissim, and Adam Smith. 2006. Calibrating Noise to Sensitivity in Private Data Analysis. In *Theory of Cryptography, Shai Halevi and Tal Rabin (Eds.)*. Springer Berlin Heidelberg, Berlin, Heidelberg, 265–284.
- Huang Fang, Xiaoyun Li, Chenglin Fan, and Ping Li. 2023. Improved Convergence of Differential Private SGD with Gradient Clipping. In *The Eleventh International Conference on Learning Representations*. <https://openreview.net/forum?id=FRLswckPXQ5>
- Jonas Geiping, Hartmut Bauermeister, Hannah Dröge, and Michael Moeller. 2020. Inverting gradients-how easy is it to break privacy in federated learning? *Advances in neural information processing systems* 33 (2020), 16937–16947.
- Niv Haim, Gal Vardi, Gilad Yehudai, michal Irani, and Ohad Shamir. 2022. Reconstructing Training Data From Trained Neural Networks. In *Advances in Neural Information Processing Systems*, Alice H. Oh, Alekh Agarwal, Danielle Belgrave, and Kyunghyun Cho (Eds.). <https://openreview.net/forum?id=Sxk8Bse3RKO>
- Moritz Hardt and Kunal Talwar. 2010. On the geometry of differential privacy. In *Proceedings of the forty-second ACM symposium on Theory of computing*. 705–714.
- Ali Hatamizadeh, Hongxu Yin, Pavlo Molchanov, Andriy Myronenko, Wenqi Li, Prerna Dogra, Andrew Feng, Mona G Flores, Jan Kautz, Daguang Xu, et al. 2023. Do gradient inversion attacks make federated learning unsafe? *IEEE Transactions on Medical Imaging* 42, 7 (2023), 2044–2056.
- Nikolas Hesse, Christoph Bodensteiner, Michael Arens, Ulrich G. Hofmann, Raphael Weinberger, and A. Sebastian Schroeder. 2018. Computer Vision for Medical Infant Motion Analysis: State of the Art and RGB-D Data Set. In *Proceedings of the European Conference on Computer Vision (ECCV) Workshops*.
- Carlos Hinojosa, Juan Carlos Niebles, and Henry Arguello. 2021. Learning Privacy-preserving Optics for Human Pose Estimation. In *2021 IEEE/CVF International Conference on Computer Vision (ICCV)*. 2553–2562. doi:10.1109/ICCV48922.2021.00257
- Andrew Howard, Mark Sandler, Grace Chu, Liang-Chieh Chen, Bo Chen, Mingxing Tan, Weijun Wang, Yukun Zhu, Ruoming Pang, Vijay Vasudevan, Quoc V.

- Le, and Hartwig Adam. 2019. Searching for MobileNetV3. In *Proceedings of the IEEE/CVF International Conference on Computer Vision (ICCV)*.
- [25] Isabel Benavente-Fernández, Simón P. Lubián-López, Syed Adil Hussain Shah Syed Taimoor Hussain Shah Lionel C. Gontard Janet Pigueiras-del Real, Angel Ruiz-Zafra. 2024. NeoVault: empowering neonatal research through a neonate data hub. *BMC Pediatrics* (2024).
- [26] Marija Jegorova, Chaitanya Kaul, Charlie Mayor, Alison Q. O’Neil, Alexander Weir, Roderick Murray-Smith, and Sotirios A. Tsaftaris. 2023. Survey: Leakage and Privacy at Inference Time. *IEEE Transactions on Pattern Analysis and Machine Intelligence* 45, 7 (2023), 9090–9108. doi:10.1109/TPAMI.2022.3229593
- [27] Aouaidja Kamel, Bin Sheng, Ping Li, Jinman Kim, and David Dagan Feng. 2020. Hybrid refinement-correction heatmaps for human pose estimation. *IEEE Transactions on Multimedia* 23 (2020), 1330–1342.
- [28] Weiwei Kong and Andres Munoz Medina. 2023. A unified fast gradient clipping framework for dp-sgd. *Advances in Neural Information Processing Systems* 36 (2023), 52401–52412.
- [29] Jonathan Lebensold, Doina Precup, and Borja Balle. 2024. On the privacy of selection mechanisms with gaussian noise. In *International Conference on Artificial Intelligence and Statistics*. PMLR, 1495–1503.
- [30] Jiefeng Li, Siyuan Bian, Ailing Zeng, Can Wang, Bo Pang, Wentao Liu, and Cewu Lu. 2021. Human pose regression with residual log-likelihood estimation. In *Proceedings of the IEEE/CVF international conference on computer vision*. 11025–11034.
- [31] Yizhuo Li, Miao Hao, Zonglin Di, Nitesh Bharadwaj Gundavarapu, and Xiaolong Wang. 2021. Test-time personalization with a transformer for human pose estimation. *Advances in Neural Information Processing Systems* 34 (2021), 2583–2597.
- [32] Yanjie Li, Sen Yang, Peidong Liu, Shoukui Zhang, Yunxiao Wang, Zhicheng Wang, Wankou Yang, and Shu-Tao Xia. 2022. Simcc: A simple coordinate classification perspective for human pose estimation. In *European Conference on Computer Vision*. Springer, 89–106.
- [33] Yanjie Li, Shoukui Zhang, Zhicheng Wang, Sen Yang, Wankou Yang, Shu-Tao Xia, and Erjin Zhou. 2021. Tokenpose: Learning keypoint tokens for human pose estimation. In *Proceedings of the IEEE/CVF International conference on computer vision*. 11313–11322.
- [34] Zheng Li, Jingwen Ye, Mingli Song, Ying Huang, and Zhigeng Pan. 2021. Online knowledge distillation for efficient pose estimation. In *Proceedings of the IEEE/CVF international conference on computer vision*. 11740–11750.
- [35] Tsung-Yi Lin, Michael Maire, Serge Belongie, James Hays, Pietro Perona, Deva Ramanan, Piotr Dollár, and C Lawrence Zitnick. 2014. Microsoft coco: Common objects in context. In *Computer Vision—ECCV 2014: 13th European Conference, Zurich, Switzerland, September 6–12, 2014, Proceedings, Part V* 13. Springer, 740–755.
- [36] Peng Lu, Tao Jiang, Yining Li, Xiangtai Li, Kai Chen, and Wenming Yang. 2024. RTMO: Towards High-Performance One-Stage Real-Time Multi-Person Pose Estimation. In *Proceedings of the IEEE/CVF Conference on Computer Vision and Pattern Recognition (CVPR)*. 1491–1500.
- [37] Haoyu Ma, Zhe Wang, Yifei Chen, Deyang Kong, Liangjian Chen, Xingwei Liu, Xiangyi Yan, Hao Tang, and Xiaohui Xie. 2022. Ppt: token-pruned pose transformer for monocular and multi-view human pose estimation. In *European Conference on Computer Vision*. Springer, 424–442.
- [38] Weian Mao, Yongtao Ge, Chunhua Shen, Zhi Tian, Xinlong Wang, Zhibin Wang, and Anton van den Hengel. 2022. Poseur: Direct human pose regression with transformers. In *European conference on computer vision*. Springer, 72–88.
- [39] Ilya Mironov. 2017. Rényi differential privacy. In *2017 IEEE 30th computer security foundations symposium (CSF)*. IEEE, 263–275.
- [40] Xuecheng Nie, Jiashi Feng, Jianfeng Zhang, and Shuicheng Yan. 2019. Single-stage multi-person pose machines. In *Proceedings of the IEEE/CVF international conference on computer vision*. 6951–6960.
- [41] Anna Rohrbach, Marcus Rohrbach, Niket Tandon, and Bernt Schiele. 2015. A dataset for movie description. In *Proceedings of the IEEE conference on computer vision and pattern recognition*. 3202–3212.
- [42] Angel Ruiz-Zafra, Daniel Precioso, Blas Salvador, Simón P. Lubián-López, Javier Jiménez, Isabel Benavente-Fernández, Janet Pigueiras, David Gómez-Ullate, and Lionel C. Gontard. 2023. NeoCam: An Edge-Cloud Platform for Non-Invasive Real-Time Monitoring in Neonatal Intensive Care Units. *IEEE Journal of Biomedical and Health Informatics* 27, 6 (2023), 2614–2624. doi:10.1109/JBHI.2023.3240245
- [43] Reza Shokri, Marco Stronati, Congzheng Song, and Vitaly Shmatikov. 2017. Membership inference attacks against machine learning models. In *2017 IEEE symposium on security and privacy (SP)*. IEEE, 3–18.
- [44] Jonathan J Tompson, Arjun Jain, Yann LeCun, and Christoph Bregler. 2014. Joint training of a convolutional network and a graphical model for human pose estimation. *Advances in neural information processing systems* 27 (2014).
- [45] Alexander Toshev and Christian Szegedy. 2014. Deeppose: Human pose estimation via deep neural networks. In *Proceedings of the IEEE conference on computer vision and pattern recognition*. 1653–1660.
- [46] Bao Wang, Quanquan Gu, March Boedihardjo, Lingxiao Wang, Farzin Barekat, and Stanley J. Osher. 2020. DP-LSSGD: A Stochastic Optimization Method to Lift the Utility in Privacy-Preserving ERM. In *Proceedings of The First Mathematical and Scientific Machine Learning Conference (Proceedings of Machine Learning Research, Vol. 107)*, Jianfeng Lu and Rachel Ward (Eds.). PMLR, 328–351. <https://proceedings.mlr.press/v107/wang20a.html>
- [47] Chen Wang, Feng Zhang, Xiatian Zhu, and Shuzhi Sam Ge. 2022. Low-resolution human pose estimation. *Pattern Recognition* 126 (2022), 108579.
- [48] Yihan Wang, Muyang Li, Han Cai, Wei-Ming Chen, and Song Han. 2022. Lite Pose: Efficient Architecture Design for 2D Human Pose Estimation. In *Proceedings of the IEEE/CVF Conference on Computer Vision and Pattern Recognition (CVPR)*. 13126–13136.
- [49] Kan Wu, Jinnian Zhang, Houwen Peng, Mengchen Liu, Bin Xiao, Jianlong Fu, and Lu Yuan. 2022. TinyViT: Fast Pretraining Distillation for Small Vision Transformers. In *Computer Vision – ECCV 2022*, Shai Avidan, Gabriel Brostow, Moustapha Cissé, Giovanni Maria Farinella, and Tal Hassner (Eds.). Springer Nature Switzerland, Cham, 68–85.
- [50] Bin Xiao, Haiping Wu, and Yichen Wei. 2018. Simple baselines for human pose estimation and tracking. In *Proceedings of the European conference on computer vision (ECCV)*. 466–481.
- [51] Yufei Xu, Jing Zhang, Qiming Zhang, and Dacheng Tao. 2022. Vitpose: Simple vision transformer baselines for human pose estimation. *Advances in Neural Information Processing Systems* 35 (2022), 38571–38584.
- [52] Suhang Ye, Yingyi Zhang, Jie Hu, Liujuan Cao, Shengchuan Zhang, Lei Shen, Jun Wang, Shouhong Ding, and Rongrong Ji. 2023. Distilpose: Tokenized pose regression with heatmap distillation. In *Proceedings of the IEEE/CVF Conference on Computer Vision and Pattern Recognition*. 2163–2172.
- [53] Da Yu, Saurabh Naik, Arturs Backurs, Sivakanth Gopi, Huseyin A Inan, Gautam Kamath, Janardhan Kulkarni, Yin Tat Lee, Andre Manoel, Lukas Wutschitz, et al. 2021. Differentially private fine-tuning of language models. *arXiv preprint arXiv:2110.06500* (2021).
- [54] Lei Yu, Ling Liu, Calton Pu, Mehmet Emre Gursoy, and Stacey Truex. 2019. Differentially private model publishing for deep learning. In *2019 IEEE symposium on security and privacy (SP)*. IEEE, 332–349.
- [55] Yuhui Yuan, Rao Fu, Lang Huang, Weihong Lin, Chao Zhang, Xilin Chen, and Jingdong Wang. 2021. Hrformer: High-resolution vision transformer for dense predict. *Advances in neural information processing systems* 34 (2021), 7281–7293.
- [56] Idris Zakariyya, Linda Tran, Kaushik Bhargav Sivangi, Paul Henderson, and Fani Deligianni. 2025. Differentially Private Integrated Decision Gradients (IDG-DP) for Radar-based Human Activity Recognition. In *IEEE/CVF Winter Conference on Applications of Computer Vision (WACV)*.
- [57] Feng Zhang, Xiatian Zhu, Hanbin Dai, Mao Ye, and Ce Zhu. 2020. Distribution-aware coordinate representation for human pose estimation. In *Proceedings of the IEEE/CVF conference on computer vision and pattern recognition*. 7093–7102.
- [58] Shihao Zhang, Baohua Qiang, Xianyi Yang, Xuekai Wei, Ruidong Chen, and Lirui Chen. 2023. Human Pose Estimation via an Ultra-Lightweight Pose Distillation Network. *Electronics* 12, 12 (2023), 2593.
- [59] Ce Zheng, Wenhan Wu, Chen Chen, Taojiannan Yang, Sijie Zhu, Ju Shen, Nasser Kehtarnavaz, and Mubarak Shah. 2023. Deep learning-based human pose estimation: A survey. *Comput. Surveys* 56, 1 (2023), 1–37.
- [60] Xingyi Zhou, Dequan Wang, and Philipp Krähenbühl. 2019. Objects as points. *arXiv preprint arXiv:1904.07850* (2019).
- [61] Yingxue Zhou, Steven Wu, and Arindam Banerjee. 2021. Bypassing the Ambient Dimension: Private {SGD} with Gradient Subspace Identification. In *International Conference on Learning Representations*. <https://openreview.net/forum?id=7dpmlkBuJFC>
- [62] Yingxue Zhou, Zhiwei Steven Wu, and Arindam Banerjee. 2020. Bypassing the ambient dimension: Private sgd with gradient subspace identification. *arXiv preprint arXiv:2007.03813* (2020).
- [63] Ligeng Zhu, Zhijian Liu, and Song Han. 2019. Deep leakage from gradients. *Advances in neural information processing systems* 32 (2019).

Received 20 February 2007; revised 12 March 2009; accepted 5 June 2009